

Spiral phase filtering and orientation-selective edge detection/enhancement

Guohai Situ,* Giancarlo Pedrini, and Wolfgang Osten

Institut für Technische Optik, Universität Stuttgart, Pfaffenwaldring 9, 70569 Stuttgart, Germany

*Corresponding author: ghsitu@gmail.com

Received January 30, 2009; revised May 11, 2009; accepted June 16, 2009;
posted June 23, 2009 (Doc. ID 106948); published July 14, 2009

A spiral phase plate with an azimuthal structure $\exp[i\phi]$ ($0 \leq \phi < 2\pi$) has been used as a filter in a $4f$ system to achieve edge enhancement. Generally such edge-enhanced effect is isotropic, i.e., each edge of an input pattern is enhanced to the same degree regardless of its orientation. We found that one can achieve anisotropic edge enhancement by breaking down the symmetry of the filtering process. This can be done in two ways: first, by use of a fractional spiral phase filter (SPF) with a fractional topological charge and a controllable orientation of the edge discontinuity, and second, by the lateral shifting of the SPF. We interpret this process as a vortex formation due to the diffraction of the Fourier spectrum of the input pattern by a SPF with an integer and fractional topological charge. Optical experiments using a spatial light modulator were carried out to verify our proposal. © 2009 Optical Society of America

OCIS codes: 100.2980, 070.6110, 050.4865, 070.6120.

1. INTRODUCTION

The spiral phase plate (SPP) with an azimuthal structure $\exp[in\phi]$, where the topological charge n is an integer and $0 \leq \phi < 2\pi$, is a common device to generate helical wavefronts, or vortex beams [1–4]. Light beams with this phase structure carry orbital angular momentum of $n\hbar$ per photon [5]. This property has gained widespread interest in many areas such as the rotation of micro-particles [6] and quantum entanglement of photons [7]. The simplest SPP with $n=1$ can also be used as a spatial filter in a $4f$ system to achieve edge enhancement [8–11], to reconstruct phase [12], to improve microscopy in optical [13–15] and soft x-ray regimes [16], and to generate dark hollow beams [17]. The applicability of the SPP in these areas relies on the curious fact that its phase is radially symmetric, i.e., the phase of the SPP depends linearly on the azimuthal angle and not at all on the radius, with a phase discontinuity at the interface of 0° and 360° . Then there is a 180° phase difference at a symmetric position in any radial line with respect to the origin. This characteristic also gives spiral phase filtering the name *radial Hilbert transform* [8,9].

Edge enhancement is a useful technique to detect the edge and shape of an object and therefore is frequently used, e.g., in industrial inspection [18–21] and fingerprint identification [22,23]. In general the edge-enhanced effect is isotropic, i.e., each edge of the input pattern is enhanced regardless of its orientation. In applications where the local features of some edges are of more interest than those of others, anisotropic edge enhancement techniques should be employed to emphasize these edges. Anisotropic edge enhancement can be done, for example, by use of anisotropic filters [22,23]. Davis *et al.* have experimentally demonstrated that this can be achieved by using fractional derivatives [24], or by interfering the zeroth- and first-order diffractions of the input image by

an acousto-optic modulator located at the Fourier plane in a $4f$ system [25]. The fractional Hilbert transform [9,26,27] is another method based on the generalization of the Hilbert transform by, for example, modifying the phase difference from π to $p\pi$, where the topological charge p is generally a noninteger whose absolute value is less than 2. One can then decide to enhance either the left- or right-hand edges by setting the value of p .

In the first proposal of the radial Hilbert transform [8,9] the authors regarded the spiral phase as an isotropic generalization of the one-dimensional (1D) signum function to two dimensions. However, it is not clear at this point why the edge enhancement takes place only in a specific direction. Recent studies [28–34] have shown that this extension is not trivial at all from both the classical and quantum optics point of view. The generalization of the topological charge from integers to fractional numbers results in a significant change in the vortex structure, which we believe affects the filtering process.

In this paper we propose to interpret the spiral phase filtering as the formation of the vortex due to the diffraction of the Fourier spectrum of an input pattern. We find that anisotropic edge detection/enhancement can be achieved by breaking down the symmetry of the filtering process. We introduce two methods to do this, that is, breaking down the symmetry (1) of the spiral phase filter with a topological charge p and an orientation angle of the edge discontinuity or the starting orientation ϑ , and (2) of the filtering by laterally shifting the singularity of the filter away from the peak of the Fourier spectrum of the input pattern to a position (ρ_0, θ) . In the first method, the degree and orientation of edge enhancement are controlled by p and ϑ ; in the second method, they are controlled by ρ_0 and θ , respectively.

In Section 2 we present an analysis of spiral phase filtering and show how the symmetry breakdown of the fil-

tering process affects the edge enhancement. This is experimentally demonstrated by use of a liquid crystal display (LCD) located at the Fourier plane in a $4f$ system to display the spiral phase. The experimental setup is presented in Section 3 and the results are shown in Section 4. Finally a conclusion is drawn in Section 5.

2. SPIRAL PHASE FILTERING AS VORTEX FORMATION

We begin with a general case of filtering by use of a spiral phase filter (SPF), i.e.,

$$\psi_n(\rho, \phi, \vartheta) = \exp[in(\phi + \vartheta)], \quad (1)$$

where ϑ is a constant angle denoting the orientation of the edge of discontinuity with respect to the positive ξ axis. A plane wave of wavelength λ is used to illuminate the input pattern $g(x,y)$ located at the front focal plane of a lens, say L1. In its rear focus plane, we obtain its Fourier spectrum written as

$$G(\rho, \phi) = G(\xi, \eta) = \mathcal{F}\{g(x,y)\}, \quad (2)$$

where

$$\xi = \rho \cos \phi, \quad \eta = \rho \sin \phi, \quad (3)$$

the symbol $\mathcal{F}\{\cdot\}$ denotes the Fourier transform, and (ξ, η) and (ρ, ϕ) denote the Cartesian and polar coordinates, respectively, of the Fourier plane. We assume that the radius R of the SPF $\psi_n(\rho, \phi)$ is greater than that of $G(\rho, \phi)$, and so we can write the field after the SPP as

$$G(\rho, \phi) = G(\rho, \phi) \psi_n(\rho, \phi, \vartheta). \quad (4)$$

If $\mathcal{G}(\rho, \phi)$ is also located at the front focus plane of a second lens L2 in a $4f$ system, we obtain at its rear focal plane an edge-enhanced version of the input image,

$$\tilde{g}(r, \varphi) = \mathcal{F}\{\mathcal{G}(\rho, \phi)\} = g(r, \varphi) \otimes \mathcal{F}\{\psi_n(\rho, \phi, \vartheta)\}, \quad (5)$$

where (r, φ) is the representation of (x, y) in polar coordinates, and the symbol \otimes denotes convolution. According to Eq. (5), to understand how the edge enhancement occurs we need to analyze the Fourier transform of the spiral phase filter, which acts as the point spread function (psf) of the system. We will show below that its distribution depends on the phase structure of the SPF.

A. Isotropic Filtering

We begin with the calculation of propagation of a plane wave of wavelength λ modulated with a spiral phase. Since we have assumed the Fourier spectrum of the input image $G(\rho, \phi)$ is insignificant when $\rho > R$, we must take the SPF to be of finite size. The field obtained at a distance z away from the SPF can be written according to the Fresnel transform

$$\begin{aligned} u'_n(\rho', \phi', \vartheta, z) &= \frac{-ik}{2\pi z} \exp\left[\frac{ik}{2z}\rho'^2\right] \\ &\times \int_0^R \int_0^{2\pi} \exp[in(\phi + \vartheta)] \exp\left(\frac{ik}{2z}\rho^2\right) \\ &\times \exp\left[-\frac{ik}{z}\rho\rho' \cos(\phi - \phi')\right] \rho d\rho d\phi, \end{aligned} \quad (6)$$

where $k = 2\pi/\lambda$ is the wave number. Equation (6) can be simplified using the Jacobi–Anger expansion [35]

$$\exp(i\rho \cos \phi) = \sum_{m=-\infty}^{\infty} i^m J_m(\rho) \exp(im\phi), \quad (7)$$

where $J_m(\rho)$ is the m th-order Bessel function of the first kind. Then we have

$$\begin{aligned} u'_n(\rho', \phi', \vartheta, z) &= \frac{(-i)^{n+1}k}{z} \exp\left[in(\phi' + \vartheta) + \frac{ik}{2z}\rho'^2\right] \\ &\times \int_0^R \exp\left(\frac{ik}{2z}\rho^2\right) J_n\left(\frac{k}{z}\rho\rho'\right) \rho d\rho, \end{aligned} \quad (8)$$

in which the integral

$$\int_0^{2\pi} \exp[i(n-m)\phi] d\phi = 2\pi \delta_{nm}, \quad (9)$$

where δ_{nm} as Kronecker's delta has been applied. Computation results show that the field u'_n is strongly radial-symmetric. Although there is a step discontinuity in the orientation ϑ , the phase of the SPF as well as the induced vortex is continuous except for the vortex core. Of more interest is that at the origin where $\rho' = 0$, $u'_n(\rho' = 0, \phi', z) = 0$ for any $z > 0$ [31]. This vortex is formed behind the SPF and its position remains stable on propagation.

In the filtering process, the actual illumination is not a plane wave but the complex Fourier spectrum of the input pattern $G(\rho, \phi)$, which usually has an extremely strong zeroth-order component located at the origin in the case of the phase of $g(x,y)$ being constant. To understand what actually takes place in the filter plane, it is better to write $G(\rho, \phi)$ in the form of

$$G(\rho, \phi) = G(\rho=0, \phi) + G(\rho \neq 0, \phi), \quad (10)$$

where $G(\rho=0, \phi)$ is the zeroth-order component of $G(\rho, \phi)$, and $G(\rho \neq 0, \phi)$ represents the other frequency components. If the filter is carefully aligned so that $G(\rho=0, \phi)$ hits the singularity, whose position, as mentioned above, remains stable on propagation, the zero-frequency component is “filtered” out, while the higher components experience spiral phase modulation. This modulation eventually forms a vortex.

As the vortex propagates to the output plane of the $4f$ system, its background becomes $g(x,y)$ due to the Fourier transform. As shown in Eq. (5), the vortex then can be written in the form of the convolution between $g(x,y)$ and $u'_n(\rho', \phi', \vartheta, \infty)$, in which the two quadratic phase factors reduce to unity. Then Eq. (8) is reduced to

$$u_n(r, \varphi, \vartheta) = \frac{(-i)^{|n|+1} k}{f} \exp[in(\varphi + \vartheta)] \int_0^R J_{|n|} \left(\frac{k r \rho}{f} \right) \rho d\rho, \quad (11)$$

where f is the focal length of the lens and the equality

$$u_n(r, \varphi, \vartheta) = \frac{(-i)^{|n|+1} f \exp[in(\varphi + \vartheta)]}{k r^2} \times \begin{cases} |n| \left[\tau \int_0^R J_0(\tau \rho) d\rho - 2 \sum_{m=0}^{\kappa-1} J_{2m+1}(\tau R) \right] - \tau R J_{|n|-1}(\tau R), & \text{if } |n| = 2\kappa + 1 \\ |n| \left[1 - J_0(\tau R) - 2 \sum_{m=1}^{\kappa} J_{2m}(\tau R) \right] - \tau R J_{|n|-1}(\tau R), & \text{if } |n| = 2\kappa + 2 \end{cases}, \quad (12)$$

where $\tau = rk/f$, and [36]

$$\int_0^R J_0(\rho) d\rho = \frac{R\pi}{2} [J_1(R)H_0(R) - J_0(R)H_1(R)] + R J_0(R), \quad (13)$$

where $H_0(R)$ and $H_1(R)$ are the zeroth- and first-order Struve functions [36], respectively.

The field of $u_n(r, \varphi)$ is also radial symmetric, as shown in Fig. 1, the density plot of u_1 . Although there is an edge dislocation in the orientation ϑ , the phase of ψ_n is continuous except at the singularity $\rho=0$. So is its Fourier transform u_n . Then the image obtained at the output plane of the 4f system is written in terms of the vortex as [8]

$$\begin{aligned} \tilde{g}(r, \varphi) &= g(r, \varphi) \otimes u_1(r, \varphi, \vartheta) \\ &= -g(r, \varphi) \otimes \frac{kR\pi}{2f\tau} [J_1(\tau R)H_0(\tau R) \\ &\quad - J_0(\tau R)H_1(\tau R)] \exp[i(\varphi + \vartheta)]. \end{aligned} \quad (14)$$

Here we have shown that the effect of the SPF can be regarded as the formation of a vortex in the form of the convolution of a radial-symmetric vortex $u_1(r, \varphi, \vartheta)$ with a background pattern $g(r, \varphi)$. Note that $u_1(r, \varphi, \vartheta)$ has an important property, i.e., $u_1(r, \varphi + \pi, \vartheta) = -u_1(r, \varphi, \vartheta)$ re-

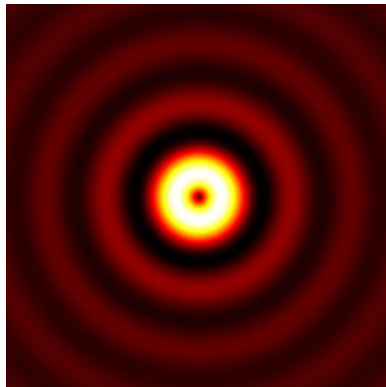


Fig. 1. (Color online) Density plot of $|u_1(r, \varphi, \vartheta)|$.

$J_{-n} = (-1)^n J_n$ has been applied to include the case for negative n . Here ρ' and φ' have been replaced by r and φ in comparison with Eq. (8) just for the sake of emphasis. Then the coordinate at the output plane is defined as $x = r \cos \varphi$, $y = r \sin \varphi$ in the Cartesian system. Now $u_n(r, \varphi)$ can be evaluated analytically as (see Appendix A for the derivation)

gardless of φ and ϑ . The convolution of it with $g(r, \varphi)$ replaces any uniform area of $g(r, \varphi)$ with zeros [13] as the effect of suppression of the zeroth-order frequency component. In addition, the filter suppresses the image points of $g(r, \varphi)$ in a symmetric environment. That is why we call this filtering isotropic.

Note that the zero-frequency component is usually located at the origin defined in the Fourier plane, so if somehow we can destroy the symmetry of the filtering process—for example, by changing the topological charge of the SPP to be a fractional number or by shifting the singularity of the filter out of the origin—then the vortex core is no longer located at the origin on propagation. As a result the zeroth-order frequency component is partly suppressed, in a manner with respect to the position of the vortex core in the far field. Then the filtered output would have a relief-like appearance. In other words by controlling the position of the vortex core it is possible to selectively “filter out” the frequency component of any order and of any lateral orientation, and thus achieve orientation-selective edge enhancement. Here we propose two methods to do this.

B. Method 1: Anisotropic Filtering Using a Fractional Spiral Phase Filter

When the topological charge p is a fractional number the phase of $\psi_p(\rho, \phi, \vartheta)$ is no longer continuous. There is a phase discontinuity in the phase along the orientation ϑ . In addition to the singularity at $\rho=0$, the wave $\psi_p(\rho, \phi, \vartheta)$ possesses an edge diffraction along this edge dislocation [28]. To understand this, we expand $\psi_p(\rho, \phi, \vartheta)$ by the Fourier series

$$\psi_p(\rho, \phi, \vartheta) = \frac{\exp(ip\pi)\sin(p\pi)}{\pi} \sum_{n=-\infty}^{\infty} \frac{\psi_n(\rho, \phi, \vartheta)}{p-n}. \quad (15)$$

Thus the Fresnel transform of $\psi_p(\rho, \phi, \vartheta)$ can be written as

$$u'_p(\rho', \phi', \vartheta, z) = \frac{\exp(ip\pi)\sin(p\pi)}{\pi} \sum_{n=-\infty}^{\infty} \frac{u'_n(\rho', \phi', \vartheta, z)}{p-n}, \quad (16)$$

where $u'_n(\rho', \phi', \vartheta, z)$ takes the form of Eq. (8). We plot the distribution of $|u'_p(\rho', \phi', \vartheta, z)|$ with $\vartheta=0$ in the vicinity of the origin when $p=0.8$ and $z=200\lambda$ in Fig. 2. It is clearly seen that the radial symmetry of the field is broken. A dark stripe appears around the $\phi'=\vartheta$ direction as a result of the interference between the diffraction fields of the singularity at the origin and of the edge phase discontinuity. Another interesting consequence of Eq. (16) is that there is no vortex at the origin of $u'_p(\rho', \phi', \vartheta, z)$, where the only nonzero contribution to the sum comes from $u'_0(\rho', \phi', \vartheta, z)$, so that

$$u'_p(\rho'_{=0}, \phi', \vartheta, z) = \frac{\exp[ip\pi]\sin(p\pi)}{p\pi} u'_0(\rho', \phi', \vartheta, z). \quad (17)$$

This means the vortex is not located at the origin $\rho'=0$ if it exists when the topological charge is not an integer. It is located at a position [28]

$$\rho' \approx 1.3293 \sqrt{\frac{8z}{k\pi}}(1-p) \quad (18)$$

when p is close to 1 and z is small (on the scale of the size of the SPF). Equation (18) shows that the position of the vortex depends on the fractional number p . Thus we can control the degree of edge enhancement by choosing the value of p .

Numerical calculation shows that the vortex is unstable on propagation when the light diffracted by the boundary of the SPF has significant contribution to the field in the vicinity of the origin. But $u'_{p,\vartheta}$ becomes stable as it propagates to the Fraunhofer domain, resulting in a field with the vortex located on a radial line orthogonal to the ϑ direction [34]. This field can be expressed as

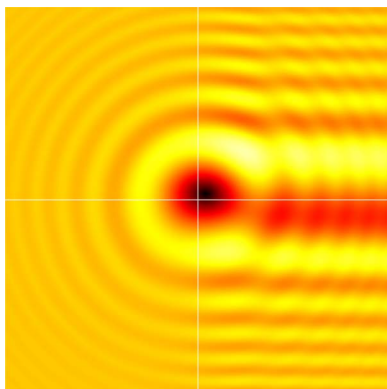


Fig. 2. (Color online) Density plots of $|u'_p(\rho', \phi', \vartheta=0, z=200\lambda)|$ with $p=0.8$ in the vicinity of the origin.

$$u_p(r, \varphi, \vartheta) = \frac{k}{2\pi f} \sum_{m=-\infty}^{\infty} (-i)^{|m|} \exp[im(\varphi + \vartheta)] \times \frac{\exp[i2\pi(p-|m|)] - 1}{p-|m|} \int_0^R J_{|m|}(\tau\rho) \rho d\rho, \quad (19)$$

where $\int_0^R J_{|m|}(\tau\rho) \rho d\rho$ can be calculated using Eqs. (A2) and (A3) below. The contribution of each $\int_0^R J_{|m|}(kr\rho/f) \rho d\rho$ component to $u_{p,\vartheta}$ clearly depends on the value of the factor

$$c_m = \left| \frac{\exp[i2\pi(p-|m|)] - 1}{p-|m|} \right|. \quad (20)$$

For a determined topological charge p , c_m is significant only when m takes the integer values close to p , especially when p approaches integer value. This can be seen in particular in Figs. 3(a)–3(c), where the distributions of c_m versus m in the cases of p equal to 0.2, 0.5, and 0.85, respectively, are plotted. So in order to evaluate $u_{p,\vartheta}$ one may sum up several terms whose subscripts are located around the closest integer of p . In the case of p being an integer, c_m reduces to Eq. (9).

Calculation results show that the radial symmetry of u_p breaks down if p is a fractional number. Figures 4(a)–4(c) show the normalized magnitude of $|u_p|$ with ϑ taking the ξ direction when $p=0.2$, 0.5, and 0.85, respectively. One can clearly see the radial asymmetry of these patterns. An interesting phenomenon is that there is no vortex associated with u_p if $p < 0.5$ as shown in Fig. 4(a). As p increases from 0, the main lobe of u_p moves along the negative y axis, and reaches a position $y \approx -1.8412f/(Rk)$ when $p=0.5$. As p passes through 0.5, a vortex is produced at the positive y axis. Then as p continuously increases, the vortex begins to move, approaching the origin along the y axis. Meanwhile the main lobe is redistributed, gradually surrounding the vortex and finally forming the familiar radial-symmetric ring pattern as p reaches 1. This process can be clearly seen from Figs. 4(b) and 4(c) and Fig. 1.

Convolving u_p with g , we obtain the filtered output

$$\tilde{g}(r, \varphi) = g(r, \varphi) \otimes u_p(r, \varphi, \vartheta). \quad (21)$$

As discussed above, when $p < 0.5$ there is no vortex in u_p , nor in \tilde{g} as a consequence. This means high-contrast edge enhancement is not achievable if $p < 0.5$. However, due to the asymmetry of u_p , it is still reasonable to expect an intensity gradient in $|\tilde{g}|$, running from $-y$ to $+y$ direction. The edges in the $-y$ direction therefore would be slightly more enhanced. When $p \geq 0.5$, the vortex in u_p , and so in \tilde{g} , is produced. High-contrast edge enhancement is therefore achieved. But this edge enhancement is anisotropic since the vortex is not located at the origin. Intensity gradients are found in $|\tilde{g}|$, running from all directions to the vortex. As seen in Fig. 4 it is expected that the edges in the $-y$ orientation are brighter than those in the $+y$ direction, which means the orientation of enhancement φ_e runs in the $\pi/2$ direction. The contrast between them decreases as the vortex moves toward the origin, which can be controlled by setting the p value from 0.5 to 1. Thus

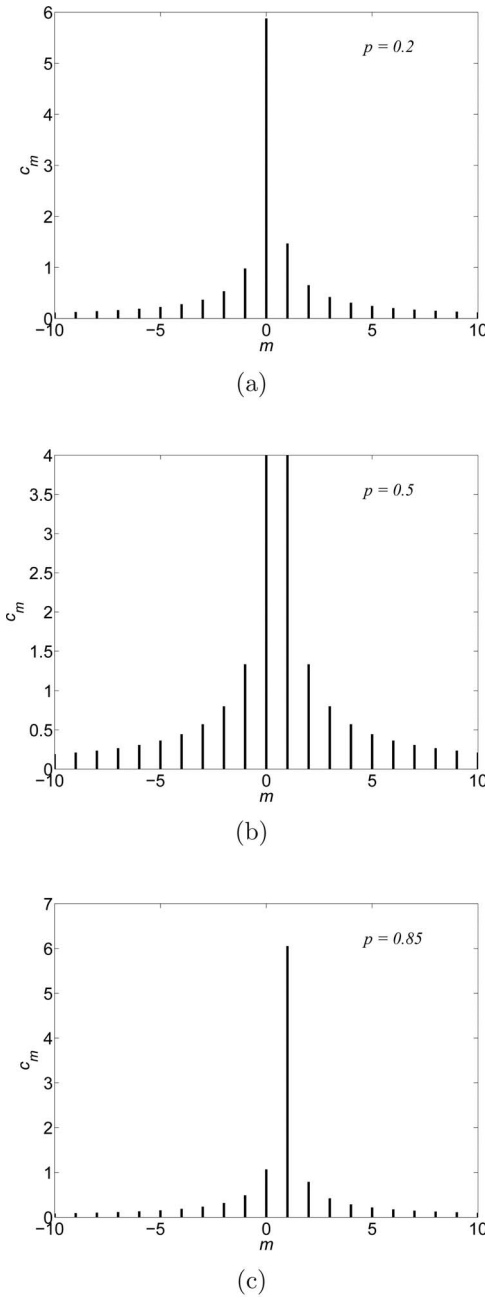


Fig. 3. Value of c_m versus m : $p =$ (a) 0.2, (b) 0.5, (c) 0.85.

the degree of enhancement can be controlled by the value of p .

As mentioned above, the orientation of the vortex in u_p is determined by ϑ , the orientation of the edge discontinuity, i.e., it appears in a radial line laterally orthogonal to ϑ . As an example we present in Fig. 5 the density plot of $|u_p|$ with $p=0.5$ and $\vartheta=-\pi/2$. It is clearly seen that the vortices are rotated anticlockwise through the angle of $-\pi/2$ with respect to Fig. 4(b).

The above analysis indicates that using the parameters $p \in [0.5, 1]$ and ϑ , we can determine the distribution of u_p , or more specifically, the position of the vortex. This is of particular convenience when using a commercially available spatial light modulator (SLM) whose phase modulation depth is usually within $[0, 2\pi]$ to represent the SPF.

For example, if we need to enhance the edges of g in the $-y$ direction to a specific degree, we only need to rotate the spiral phase displaced on the SLM through π .

C. Method 2: Anisotropic Filtering by Shifting the Full-Range Spiral Phase Filter

The other way we propose here to break the symmetry of the filtering process is to shift the singularity of the full-range SPF away from the origin to a position specified by (ρ_0, θ) , where $\rho_0 < R$ and $\theta \in [0, 2\pi]$ in polar coordinates. In this case the SPF can be written as

$${}_s\psi_1(\rho, \phi, \rho_0, \theta) = \frac{\rho \exp(i\phi) + \rho_0 \exp(i\theta)}{\sqrt{\rho^2 + \rho_0^2 + 2\rho\rho_0 \cos(\phi - \theta)}}, \quad (22)$$

where the subscript s stands for *shift*. Substituting Eq. (22) into Eq. (6) and applying the Jacobi–Anger expansion we obtain

$$\begin{aligned} {}_su'_1(\rho', \phi', \rho_0, \theta, z) = & A(\rho', z)\rho_0 \exp(i\theta) \\ & \times \int_0^R J_0\left(\frac{k}{z}\rho'\rho\right) B(\rho, z, \rho_0, \theta)\rho d\rho - iA(\rho', z) \\ & \times \exp(i\phi') \int_0^R \rho J_1\left(\frac{k}{z}\rho'\rho\right) B(\rho, z, \rho_0, \theta)\rho d\rho, \end{aligned} \quad (23)$$

where

$$A(\rho', z) = -\frac{ik}{2\pi z} \exp\left(\frac{ik}{2z}\rho'^2\right) \quad (24)$$

and

$$\begin{aligned} B(\rho, z, \rho_0, \theta) = & \frac{2}{\rho + \rho_0} \left[F\left(\frac{\theta}{2}, \frac{2\rho\rho_0}{(\rho + \rho_0)^2}\right) \right. \\ & \left. - F\left(\frac{\theta - 2\pi}{2}, \frac{2\rho\rho_0}{(\rho + \rho_0)^2}\right) \right] \exp\left(\frac{ik}{2z}\rho^2\right), \end{aligned} \quad (25)$$

where

$$F(\theta, m) = \int_0^\theta \frac{1}{\sqrt{1 - m \sin^2 \phi}} d\phi \quad (26)$$

is the elliptic integral of the first kind.

Although Eq. (23) is analytically unintegrable, we can see from this equation that ${}_su'_1$ is essentially an interference between a vortex beam [the one with $\exp(i\phi')$] and a nonvortex beam. As a result the vortex is not located at the origin. Numerical calculation shows that when the propagation distance z is small, a vortex is produced at the position (ρ_0, θ) , resulting in an anisotropic filtering.

The breakdown of symmetry is an important difference between this approach and isotropic filtering. When z is large, the contribution of the diffraction from the boundary of the SPF to the field in the vicinity of the vortex becomes significant. As discussed in Subsection 2.A, in the Fourier domain the complex amplitude becomes

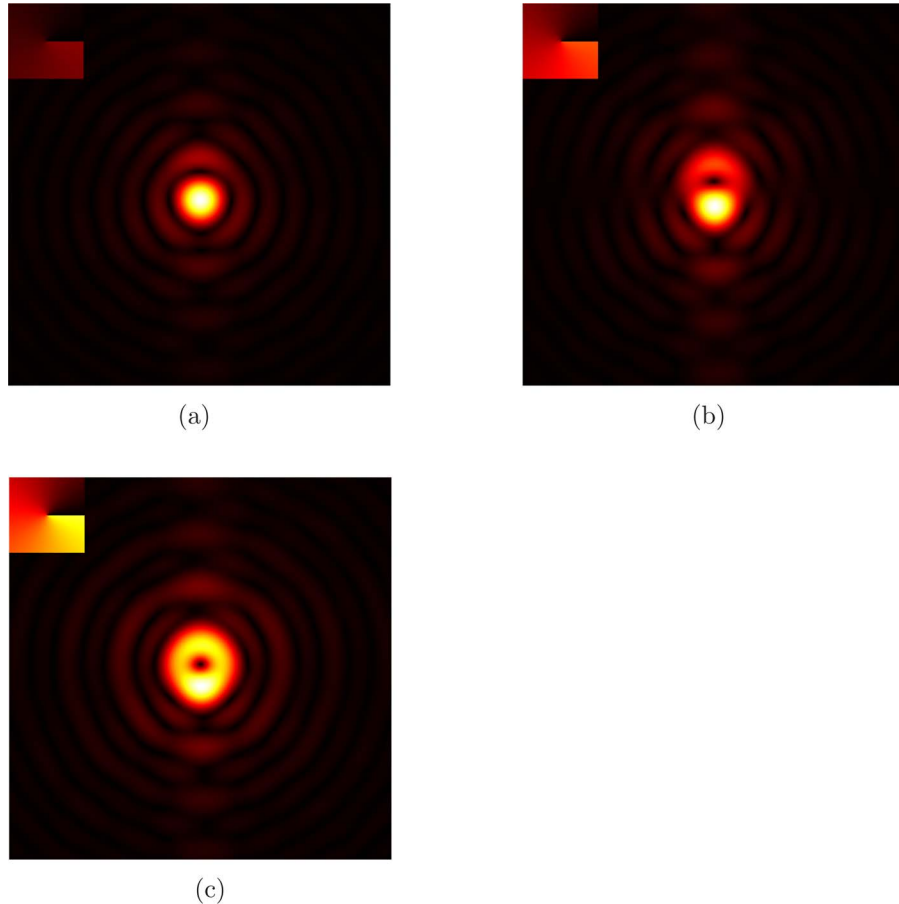


Fig. 4. (Color online) Density plots of $|u_p(r, \varphi, \theta=0)|$ with $p=(\text{a}) 0.2, (\text{b}) 0.5, (\text{c}) 0.8$. On the upper-left side of these figures we plot the status of the SPF.

$$\begin{aligned}
 {}_s u_1(r, \varphi, \rho_0, \theta, z) &= \frac{-ik}{2\pi z} \rho_0 \exp(i\theta) \\
 &\times \int_0^R J_0\left(\frac{k}{z}r\rho\right) B(\rho, z_{\infty}, \rho_0, \theta) \rho d\rho - \frac{k}{2\pi z} \\
 &\times \exp(i\varphi) \int_0^R \rho J_1\left(\frac{k}{z}r\rho\right) B(\rho, z_{\infty}, \rho_0, \theta) \rho d\rho,
 \end{aligned} \tag{27}$$

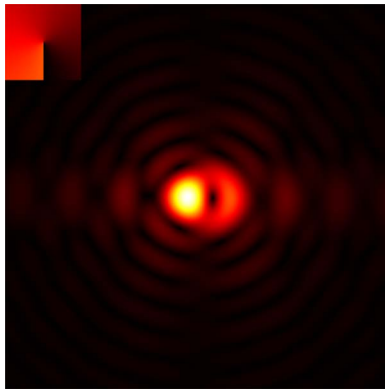


Fig. 5. (Color online) Density plot of $|u_p(r, \varphi, \theta=-\pi/2)|$ with $p=0.5$.

where B has the form of Eq. (25) without the quadratic phase factor. As a consequence, the position of the vortex changes on propagation, ending in a radial line (r_e, φ_e) laterally perpendicular to the line $\varphi=\theta$, that is,

$$\varphi_e = \theta + \frac{\pi}{2}, \tag{28}$$

where r_e is a function of ρ_0 for which we are unable to obtain an analytical expression. Equation (28) means that the position of the vortex rotates over $\pi/2$ in the far field from its original position with respect to the origin. We present a density plot of ${}_s u'_1(\varphi, r)$ in Figs. 6(a)–6(c) when $\theta=\pi/4$, the vortex orienting in the direction $\varphi=3\pi/4$. One can see that the distribution of the field is asymmetric, similar to the case when the topological charge is a fractional number. If θ rotate through an angle, φ_e will rotate through the same angle, as seen in Fig. 6(d). The distance of the vortex from the origin r_e is determined by ρ_0 . In Figs. 6(a)–6(c) we plot the magnitude of ${}_s u'_1$ with $\rho_0 = 0.2R, 0.55R$ and $0.85R$. When ρ_0 is very small, the vortex is located closed to the origin, and ${}_s u'_1$ is similar to u_1 . When ρ_0 becomes larger, the vortex moves increasingly away from the origin. Finally it disappears when ρ_0 is larger than R , where the singularity has no contribution to the field ${}_s u'_1$.

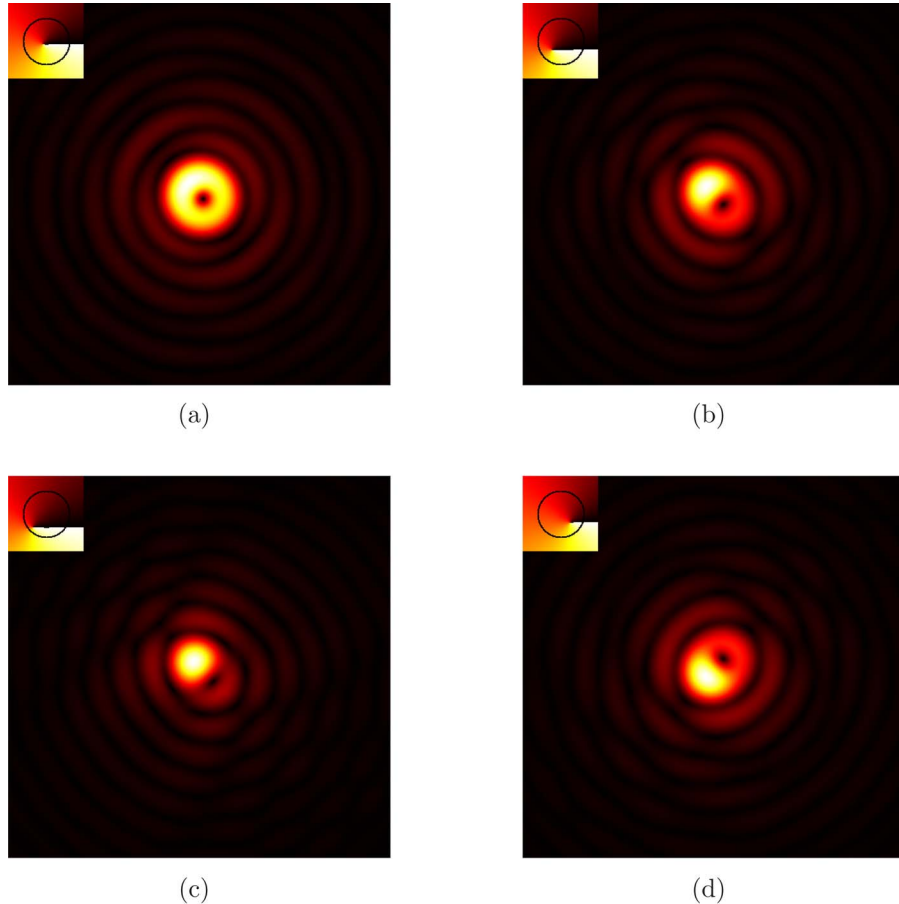


Fig. 6. (Color online) Density plot of $|_s u_1|$ with (ρ_0, θ) equal to (a) $(0.2R, \pi/4)$, (b) $(0.55R, \pi/4)$, (c) $(0.85R, \pi/4)$, (d) $(0.55R, 3\pi/4)$. On the upper-left-side of these figures we plot the status of the SPF. The dark ring in the figure is the boundary of the filter. Note that in the calculation the area of the SPF outside the boundary is zero. It is shown here just for a clearer illustration of the state of the SPF.

The filtered output \tilde{g} is a vortex, that can be expressed as the convolution between g and $_s u'_1$ as shown in Eq. (5). It is expected that \tilde{g} appears with an intensity gradient along the $+y$ direction with setting $\theta=0$, as analyzed above. As a result the edges facing the $-y$ direction receive more enhancement than those facing the $+y$ direction. Orientation edge enhancement is thus achieved. Specifically, the orientation of the edge enhancement is determined by θ , while the degree of enhancement is determined by the distance between the vortex and the origin, or ρ_0 . The closer the ρ_0 value to 0, the more symmetric the vortex and therefore the more isotropic the enhancement. On the other hand, when ρ_0 becomes larger, the degree of enhancement becomes significant at first, but if ρ_0 exceeds a specific value ρ_h the vortex disappears, i.e., there is no high-contrast enhancement in \tilde{g} . Unfortunately we are unable to find an analytical expression for ρ_h , but it may have some connection with the size of the significant area of G , the Fourier spectrum of g . Only when ρ_0 is within the area where G has significant value does the contribution of singularity in the SPF to the formation of the vortex in \tilde{g} become significant.

3. EXPERIMENT SETUP

We have carried out a proof-of-principle experiment to verify the two anisotropic spiral phase filtering methods.

The experimental setup is shown schematically in Fig. 7. A laser with a wavelength of 532 nm was used as the light source. The laser beam was first collimated, then passed through an iris aperture before being directed into the $4f$ system. The focal lengths of the lenses L1 and L2 were $f_1=160$ mm and $f_2=250$ mm, respectively. The object we used was a chrome-coated soda lime glass forming a transparent pattern composed of the letters "distr," fabricated in our institute. A reflective SLM (Holoeye LC-R 3000) was placed at the Fourier plane to displace the SPF. The LCD used was constructed as a LCOS display, which was a Brillian WUXGA LCD from Three-Five Systems. It had a resolution of 1920×1200 pixels with pixel size of $9.5 \mu\text{m} \times 9.5 \mu\text{m}$. The display had its own driver electronics and was addressed by a DVI-D-capable graphics adapter (PixelPerfect) from Imagine Graphics. The LCD

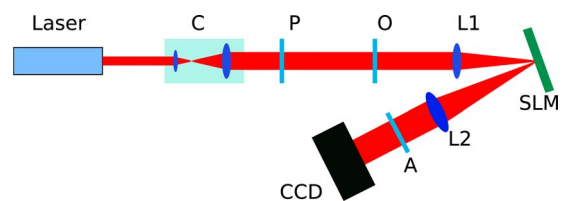


Fig. 7. (Color online) Setup of the optical experiment. A, analyzer; P, polarizer; C, collimator; O, object. The focal lengths of the Fourier lenses L1 and L2 are 160 and 250 mm, respectively.

could modulate 256 different gray levels, and the gamma curve, which gave the assignment of gray levels to the applied voltage, could be adjusted by using the software interface. To achieve pure phase modulation, a polarizer with a polarized angle of 39° with respect to the LCD was placed between the collimator and the iris, and an analyzer under 123° was placed between the CCD and L2. The SLM was therefore optimally characterized to operate in the phase mode [37]. At the rear focus plane of L2 a CCD (TELI CS3910 TV B/W) with resolution of 1300×1030 pixels whose dimension was $6.7 \times 6.7 \mu\text{m}$ square was used as the detector.

4. EXPERIMENTAL RESULTS

When no phase pattern was displayed on the SLM, we obtained at the CCD plane the image of the input pattern. Next we displayed a spiral phase pattern as described by Eq. (1) with the topological charge $p=1$ on the SLM. We made careful alignment so that the zero frequency component of the Fourier spectrum of the input image overlapped with the singularity of the spiral phase. The output was then an edge enhanced version of the input as shown in [9]. Note that this is an isotropic enhancement, i.e., all the edges were enhanced to the same degree regardless of their orientations as indicated by Eq. (14). If we change the value of p , it is possible to selectively enhance the edge in one direction. In the case of $0 < p < 1$ the edges on the left side are enhanced, while in the case of $1 < p < 2$ those on the right side are enhanced [26,9].

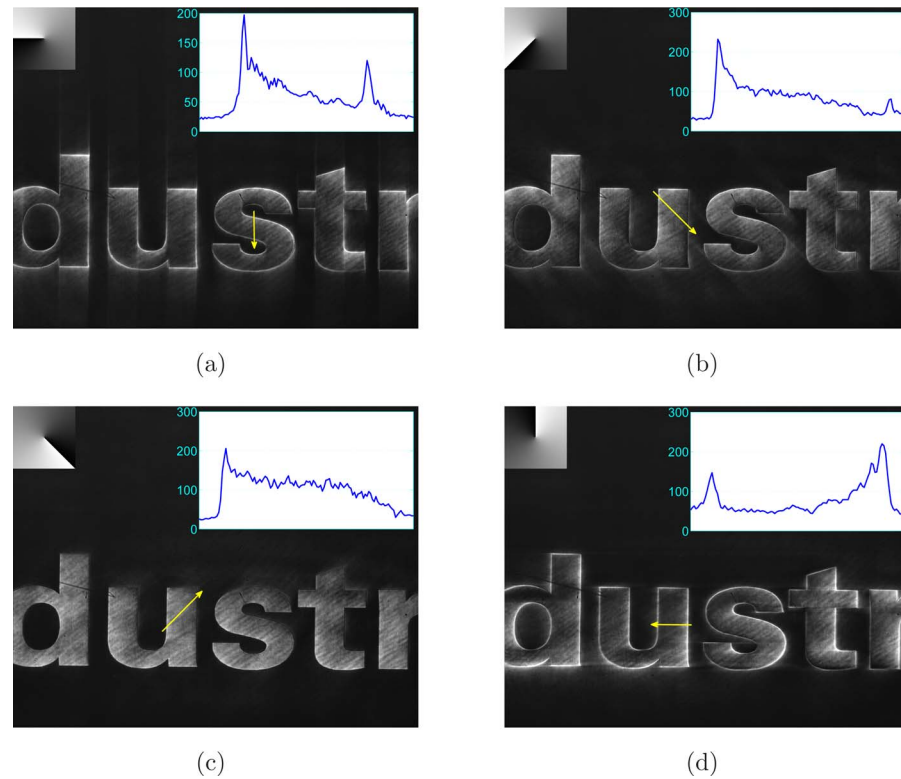


Fig. 8. (Color online) Experimental results of method 1. The (p, ϑ) values are (a) $(0.8, \pi)$, (b) $(0.6, 5\pi/4)$, (c) $(0.4, 7\pi/4)$, (d) $(0.9, \pi/2)$. It is shown that $\varphi_e = 3\pi/2, 7\pi/4, \pi/4$, and π , i.e., respectively along the arrows in (a)–(d). The stages of the SPP are shown, respectively, in the upper-left corner of these figures. The subfigures in the upper-right corners show the cross sections of the arrows and the output patterns. One can see from (c) that the filtered output appears with an intensity gradient when $p < 0.5$. High-contrast edge enhancement takes place when $p \geq 0.5$.

A. Results of Method 1

As stated in Subsection 2.B the orientation of enhancement is generally perpendicular to the line of edge discontinuity in the SPP. Thus it is possible to achieve orientation-selective edge enhancement by rotating the filter. Usually the direction of edge discontinuity ϑ is identical to the starting angle of the spiral phase when $0 < p < 1$. This angle is initially set to be 0 as the phase discontinuity occurs along the positive ξ axis. In our experiments, we set the values of ϑ at $\pi, 5\pi/4, 7\pi/4$, and $\pi/2$. One can see from the results in Figs. 8(a)–8(d), respectively, that the edge enhancement takes place at the orientation of $\varphi_e = 3\pi/2, 7\pi/4, \pi/4$, and π in the output plane, all of which rotate an angle over $\pi/2$ with respect to ϑ in each case. This verifies the theoretical calculation of Eq. (19) shown in Fig. 4(b) and Fig. 5. The value of p in Figs. 8(a)–8(d) was set to 0.8, 0.6, 0.4, and 0.9, respectively. This can be noted by the difference of edge-enhanced contrast along φ_e . One other important result presented here is that, as analyzed in Subsection 2.B, there is no significant edge enhancement in Fig. 8(c) when $p < 0.5$ and is therefore insufficient to produce a vortex. To obtain high-contrast edge enhancement, one should set the p value around 0.8, or at least larger than 0.5.

B. Results of Method 2

Asymmetric spiral phase filtering is optically implemented using the same setup as described above, with $p = 1$ in this case. Figures 9(a)–9(d) show the output when the SPF is shifted to the coordinate $(\rho_0, \theta) = (3\delta, \pi/2)$,

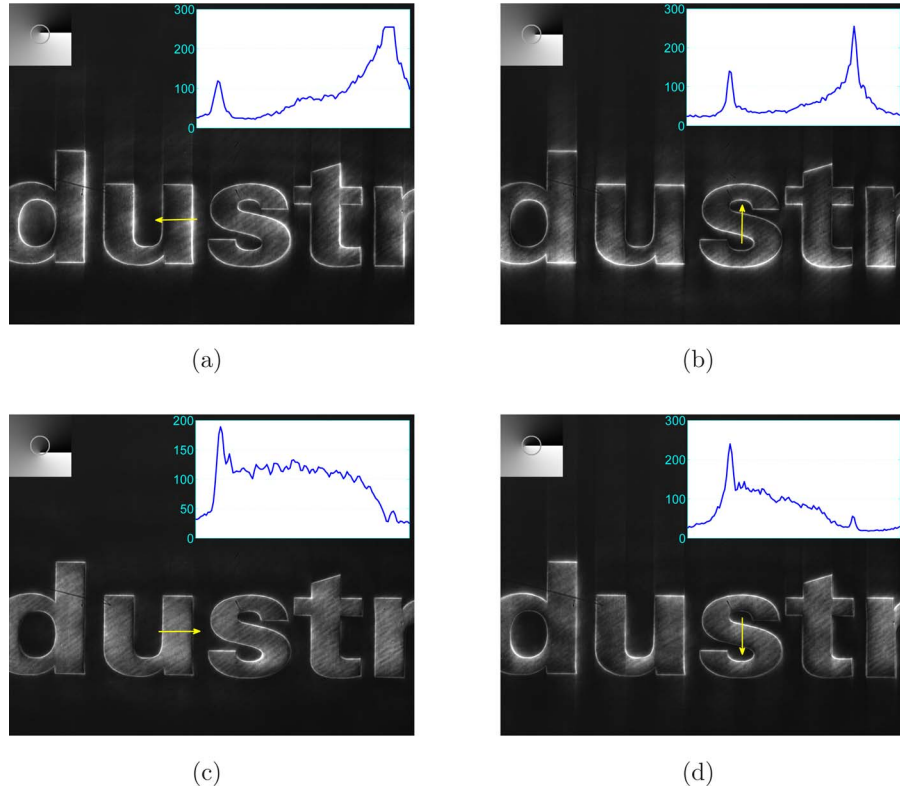


Fig. 9. (Color online) Experimental results of method 2. The (ρ_0, θ) values are (a) $(3\delta, \pi/2)$, (b) $(6\delta, 0)$, (c) $(11\delta, 3\pi/2)$, (d) $(10\delta, \pi)$, where $\delta=9.5 \mu\text{m}$ is the pixel dimension of the LCD. It is shown in these figures that $\varphi_e=\pi, \pi/2, 0$, and $3\pi/2$, i.e., respectively along the arrows in (a)–(d). The stages of the SPP are shown, respectively, in the upper-left corner of these figures. The subfigures in the upper-right corners show the cross sections of the arrows and the output patterns. The stages of the SPP are shown, respectively, in the upper-left corner of these figures.

$(6\delta, 0)$, $(11\delta, 3\pi/2)$, and $(10\delta, \pi)$, where $\delta=9.5 \mu\text{m}$ is the pixel dimension of the LCD, with respect to the origin. One can clearly see that the edge enhancement in these figures takes place at the orientations $\varphi_e=\theta+\pi/2=\pi, \pi/2, 0$, and $3\pi/2$, respectively, as theoretically calculated using Eq. (23) in Fig. 6. The edges in the selected orientation are enhanced with high contrast when ρ_0 is small. In comparison with the case of isotropic filtering, the intensity in this case exhibits a gradient distribution along the orientation of edge enhancement. However when ρ_0 becomes large enough, the enhancement becomes insignificant, as shown in Figs. 9(c) and 9(d).

5. CONCLUSION

We have found that anisotropic edge detection/enhancement can be achieved by breaking down the symmetry of the filtering process of a SPP in a $4f$ system. We have shown that this can be done by either a fractional- or a full-range SPF displayed on a SLM located in the Fourier plane. In the first method, the orientation is controlled by the direction of phase discontinuity ϑ and the degree of enhancement is controlled by the value of the topological charge p . In method 2, these two parameters are specified by the position of the singularity. We have optically generated the SPF using a reflective SLM and experimentally demonstrated our proposal. The experimental results have also been verified by numerical calculations.

One can see that when p is small or ρ_0 is large, the filtered output presents some shadow effect, which is useful in microscopy of phase objects [14] and will be studied in a following contribution.

APPENDIX A: DERIVATION OF EQ. (12)

Recalling the recurrence relation

$$\frac{d}{dp}[\rho^{-|n|}J_{|n|}(\rho)] = -\rho^{-|n|}J_{|n|+1}(\rho), \quad (\text{A1})$$

we have

$$\int_0^R J_{|n|}(\rho) \rho d\rho = |n| \int_0^R J_{|n|-1}(\rho) d\rho - R J_{|n|-1}(R). \quad (\text{A2})$$

The first term on the right-hand side of Eq. (30) then can be evaluated as [36]

$$\begin{aligned} & \int_0^R J_{|n|-1}(\rho) d\rho \\ &= \begin{cases} \int_0^R J_0(\rho) d\rho - 2 \sum_{m=0}^{\kappa-1} J_{2m+1}(R), & \text{if } |n|=2\kappa+1 \\ 1 - J_0(R) - 2 \sum_{m=1}^{\kappa} J_{2m}(R), & \text{if } |n|=2\kappa+2 \end{cases}, \end{aligned} \quad (\text{A3})$$

where κ is an integer. The substitution of Eqs. (A2) and (A3) into Eq. (11) eventually yields Eq. (12).

ACKNOWLEDGMENTS

G. Situ gratefully acknowledges the support of the Alexander von Humboldt Foundation. We thank Thomas Schoder for the fabrication of the input pattern and Christian Kohler for help in setting up the SLM.

RERENCES

- M. W. Beijersbergen, R. P. C. Coerwinkel, M. Kristensen, and J. P. Woerdman, "Helical-wavefront laser beams produced with a spiral phaseplate," *Opt. Commun.* **112**, 321–327 (1994).
- V. V. Kotlyar, A. A. Almazov, S. N. Khonina, V. A. Soifer, H. Elfstrom, and J. Turunen, "Generation of phase singularity through diffraction of a plane or Gaussian beam by a spiral phase plate," *J. Opt. Soc. Am. A* **22**, 849–861 (2005).
- V. V. Kotlyar, S. N. Khonina, A. A. Kovalev, V. A. Soifer, H. Elfstrom, and J. Turunen, "Diffraction of a plane, finite-radius wave by a spiral phase plate," *Opt. Lett.* **31**, 1597–1599 (2006).
- V. V. Kotlyar, A. A. Kovalev, R. V. Skidanov, O. Y. Moiseev, and V. A. Soifer, "Diffraction of a finite-radius plane wave and a Gaussian beam by a helical axicon and a spiral phase plate," *J. Opt. Soc. Am. A* **24**, 1955–1964 (2007).
- L. Allen, M. W. Beijersbergen, R. J. C. Spreeuw, and J. P. Woerdman, "Orbital angular momentum of light and the transformation of Laguerre–Gaussian laser modes," *Phys. Rev. A* **45**, 8185–8190 (1992).
- H. He, M. E. J. Friese, N. R. Heckenberg, H. Rubinsztein-Dunlop, "Direct observation of transfer of angular momentum to absorptive particles from a laser beam with a phase singularity," *Phys. Rev. Lett.* **75**, 826–829 (1995).
- A. Mair, A. Vaziri, G. Weihs, and A. Zeilinger, "Entanglement of the orbital angular momentum states of photons," *Nature (London)* **412**, 313–315 (2001).
- S. N. Khonina, V. V. Kotlyar, M. V. Shinkaryev, V. A. Soifer, and G. V. Uspleniev, "The phase rotor filter," *J. Mod. Opt.* **39**, 1147–1154 (1992).
- J. A. Davis, D. E. McNamara, D. M. Cottrell, and J. Campos, "Image processing with the radial Hilbert transform: theory and experiments," *Opt. Lett.* **25**, 99–101 (2000).
- J. A. Davis, D. E. McNamara, and D. M. Cottrell, "Analysis of the fractional Hilbert transform," *Appl. Opt.* **37**, 6911–6913 (1998).
- C.-S. Guo, Y. Zhang, Y.-J. Han, J.-P. Ding, and H.-T. Wang, "Generation of optical vortices with arbitrary shape and array via helical phase spatial filtering," *Opt. Commun.* **259**, 449–454 (2006).
- K. G. Larkin, D. J. Bone, and M. A. Oldfield, "Natural demodulation of two-dimensional fringe patterns. I. General background of the spiral phase quadrature transform," *J. Opt. Soc. Am. A* **18**, 1862–1870 (2001).
- S. Fürhapter, A. Jesacher, S. Bernet, and M. Ritsch-Marte, "Spiral phase contrast imaging in microscopy," *Opt. Express* **13**, 689–694 (2005).
- A. Jesacher, S. Fürhapter, S. Bernet, and M. Ritsch-Marte, "Shadow effects in spiral phase contrast microscopy," *Phys. Rev. Lett.* **94**, 233902 (2005).
- C. Maurer, A. Jesacher, S. Fürhapter, S. Bernet, and M. Ritsch-Marte, "Upgrading a microscope with a spiral phase plate," *J. Microsc.* **230**, 134–142 (2007).
- A. Sakdinawat and Y. Liu, "Soft-x-ray microscopy using spiral zone plates," *Opt. Lett.* **32**, 2635–2637 (2007).
- Q. Xie and D. Zhao, "Generation of dark hollow beams by using a fractional radial Hilbert transform system," *Opt. Commun.* **275**, 394–398 (2007).
- R. C. Gonzalez and R. E. Woods, *Digital Image Processing*, 2nd ed. (Prentice Hall, 2002).
- J. Xia, D. B. Dunn, T.-C. Poon, and P. P. Banerjee, "Image edge enhancement by Bragg diffraction," *Opt. Commun.* **128**, 1–7 (1996).
- D. Cao, P. P. Banerjee, and T.-C. Poon, "Image edge enhancement with two cascaded acousto-optic cells with contrapropagating sound," *Appl. Opt.* **37**, 3007–3014 (1998).
- A. Márquez, C. Neipp, A. Beléndez, S. Gallego, M. Ortúñoz, and I. Pascual, "Edge-enhanced imaging with polyvinyl alcohol/acrylamide photopolymer gratings," *Opt. Lett.* **28**, 1510–1512 (2003).
- S. Greenberg and D. Kogan, "Structure-adaptive anisotropic filter applied to fingerprints," *Opt. Eng. (Bellingham)* **44**, 127004 (2005).
- X. Chen, J. Tian, Y. Zhang, and X. Yang, "Enhancement of low quality fingerprints based on anisotropic filtering," *Lect. Notes Comput. Sci.* **3832**, 302–308 (2005).
- J. A. Davis, D. A. Smith, D. E. McNamara, D. M. Cottrell, and J. Campos, "Fractional derivatives—analysis and experimental implementation," *Appl. Opt.* **40**, 5943–5948 (2001).
- J. A. Davis and M. D. Nowak, "Selective edge enhancement of images with an acousto-optic light modulator," *Appl. Opt.* **23**, 4835–4839 (2002).
- A. W. Lohmann, D. Mendlovic, and Z. Zalevsky, "Fractional Hilbert transform," *Opt. Lett.* **21**, 281–283 (1996).
- A. W. Lohmann, E. Tepichin, and J. G. Ramirez, "Optical implementation of the fractional Hilbert transform," *Appl. Opt.* **36**, 6620–6626 (1997).
- M. V. Berry, "Optical vortices evolving from helicoidal integer and fractional phase steps," *J. Opt. A, Pure Appl. Opt.* **6**, 259–268 (2004).
- J. Leach, E. Yao, and M. J. Padgett, "Observation of the vortex structure of a non-integer vortex beam," *New J. Phys.* **6**, 71 (2004).
- W. M. Lee, X. C. Yuan, and K. Dholakia, "Experimental observation of optical vortex evolution in a Gaussian beam with an embedded fractional phase step," *Opt. Commun.* **239**, 129–135 (2004).
- J. B. Götte, S. Franke-Arnold, R. Zambrini, and S. M. Barnett, "Quantum formulation of fractional orbital angular momentum," *J. Mod. Opt.* **54**, 1723–1738 (2007).
- J. B. Götte, K. O'Holleran, D. Preece, F. Flossmann, S. Franke-Arnold, S. M. Barnett, and M. J. Padgett, "Light beams with fractional orbital angular momentum and their vortex structure," *Opt. Express* **16**, 993–1006 (2008).
- S. S. R. Oemrawsingh, A. Aiello, E. R. Eliel, G. Nienhuis, and J. P. Woerdman, "How to observe high-dimensional two-photon entanglement with only two detectors," *Phys. Rev. Lett.* **92**, 217901 (2004).
- I. V. Basistiy, V. A. Pas'ko, V. V. Slyusar, M. S. Soskin, and M. V. Vasnetsov, "Synthesis and analysis of optical vortices with fractional topological charges," *J. Opt. A, Pure Appl. Opt.* **6**, S166–S169 (2004).
- G. B. Arfken and H. J. Weber, *Mathematical Methods For Physicists*, 5th ed. (Academic, 2001).
- M. Abramowitz and I. A. Stegun, *Handbook of Mathematical Functions with Formulas, Graphs, and Mathematical Tables* (Dover, 1970).
- C. Kohler, X. Schwab, and W. Osten, "Optimally tuned spatial light modulators for digital holography," *Appl. Opt.* **45**, 960–967 (2006).